Radiat Med (2006) 24:538–544
DOI 10.1007/s11604-006-0054-x

MINIREVIEW

# Usefulness of fully automated constant ROI analysis software for the brain: 3DSRT and FineSRT

**Ryo Takeuchi · Tami Sengoku · Kaname Matsumura**

Accepted: February 22, 2006


**Abstract** The positioning or selection of a region of interest (ROI) is an essential step for the quantification of brain images. However, so long as the ROIs were manually selected, results obtained fluctuated considerably with subtle changes in their positioning. To perform an ROI analysis of the brain with improved objectivity and excellent reproducibility, we recently established fully automated ROI-based analysis software for the brain, the so-called 3DSRT and the FineSRT. 3DSRT performed by consecutive analyzing process as follows: (1) anatomical standardization using the SPM99 algorithm; (2) analysis using constant 318 ROIs divided into 12 groups (segments) on each hemisphere; (3) calculation of the area-weighted average for each of the respective 24 segments; (4) display of the results followed by the saving of respective values of the 636 ROIs (both hemispheres). The processes of the FineSRT were fundamentally similar to that of 3DSRT, but on FineSRT more precise constant 1394 ROIs (both hemispheres) corresponding to the respective cerebral convolutions were used. Our programs have been useful for objective estimation of cerebrovascular reserve, especially for follow-up studies of an infant with moyamoya disease, because we could compare the results without consideration of the patient's growth during the follow-up period.

R. Takeuchi (✉)
Shizuoka PET Imaging Center, 4-27-1 Kita-anndoh, Aoi-ku, Shizuoka 420-8527, Japan
Tel. +81-54-247-6111 (ext. 8005); Fax +81-54-247-6140
e-mail: roytkuc@general-hosp.pref.shizuoka.jp

T. Sengoku · K. Matsumura
Division of PET Diagnosis, Department of Radiology, Higashitemma Clinic, Osaka, Japan

This work was presented as an educational lecture at the 64th Japan Radiological Society meeting, Yokohama, April 2005.

## Introduction

Voxel-based analysis software such as SPM[1,2] and 3DSSP[3] has been widely used for the objective analysis of brain images with various imaging drugs. Those software packages compared the differences of two anatomically standardized groups with the linear model at each voxel. Although they were effective for the statistical analysis of regional cerebral blood flow (CBF) changes, their unsuitability for the quantification of the regional CBF values were noticeable owing to the positioning or selection of the region of interest (ROI), an essential step for the quantification of brain images. So long as the ROIs were manually selected, the results obtained fluctuated considerably with subtle changes in their positioning, and overlooking important information in an area on which ROI was not set was possible. To perform an ROI analysis of the brain with improved objectivity and excellent reproducibility, we are introducing our recently established fully automated ROI-based analysis software for the brain, the 3DSRT[4–6] and the FineSRT.[7] Along with the basis of the fully automated ROI-based analysis software, we present a representative case to demonstrate the usefulness of our new software.

## Methods

### Analyzing processes of 3DSRT and FineSRT

The consecutive analyzing fast process of 3DSRT is as follows.

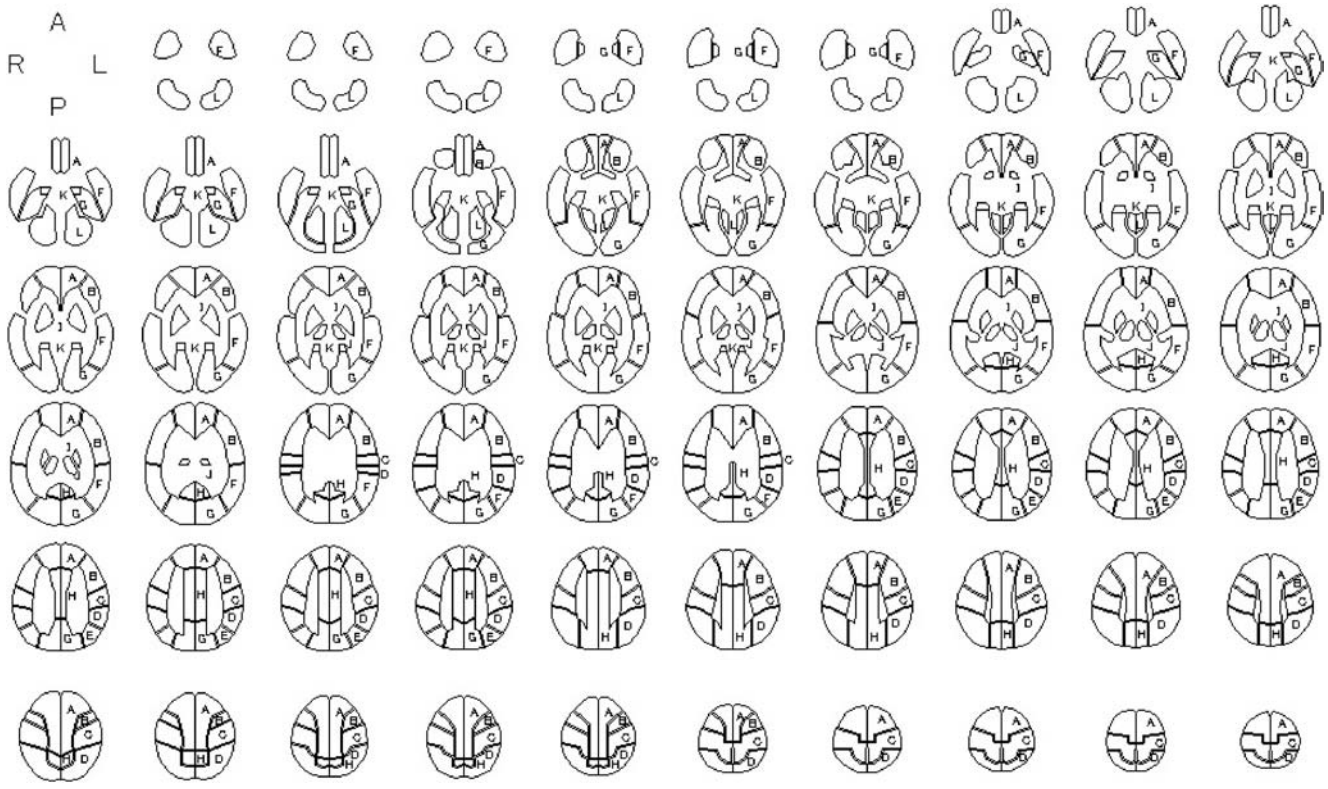


**Fig. 1.** Constant 636 regions of interest (ROIs) (318 ROIs on each hemisphere) for the 3DSRT. *A*, callosomarginal; *B*, precentral; *C*, central; *D*, parietal; *E*, angular; *F*, temporal; *G*, posterior cerebral; *H*, pericallosal; *I*, basal ganglia; *J*, thalamus; *K*, hippocampus; *L*, cerebellum

1. Anatomical standardization using the SPM99[8] algorithm
2. Analysis using constant 318 ROIs divided into 12 groups (segments) on each hemisphere
3. Calculation of the area-weighted average for each of the respective 24 segments based on the value in each ROI
4. Display of the results followed by the saving of respective values of the 636 ROIs (both hemispheres) as the CSV file format

For the 3DSRT analysis, a constant 318 ROIs on each brain hemisphere were prepared. The constant ROIs were determined on the T1-weighted magnetic resonance (MR) images anatomically standardized by SPM99 and classified into 12 segments according to their arterial supply as follows.

1. Callosomarginal, 53 ROIs;
2. Precentral, 43 ROIs
3. Central, 28 ROIs
4. Parietal, 28 ROIs
5. Angular, 8 ROIs
6. Temporal, 35 ROIs
7. Posterior cerebral, 40 ROIs
8. Pericallosal, 31 ROIs
9. Basal ganglia, 14 ROIs
10. Thalamus, 10 ROIs
11. Hippocampus, 15 ROIs
12. Cerebellum, 13 ROIs (Fig. 1).

The processes using the FineSRT were fundamentally similar to those of 3DSRT, but for the FineSRT analysis a larger number of constant ROIs were produced by the subdivision of each ROI of 3DSRT to correspond to the respective cerebral convolutions. Thus, the constant ROIs of FineSRT analysis on each brain hemisphere were composed of 697 ROIs grouped into 42 groups (subsegments) (total of 1394 for both hemispheres) as follows.

1. Callosomarginal, 138 ROIs: superior frontal 46, medial frontal 48, paracentral lobule 10, anterior cingulate 20, subcallosal 3, orbital 6, rectal 5
2. Precentral, 70 ROIs: middle frontal 42, inferior frontal 28
3. Central, 56 ROIs: precentral 28, postcentral 28
4. Parietal, 49 ROIs: superior parietal 16, inferior parietal 25, supramarginal 8
5. Angular, 8ROIs

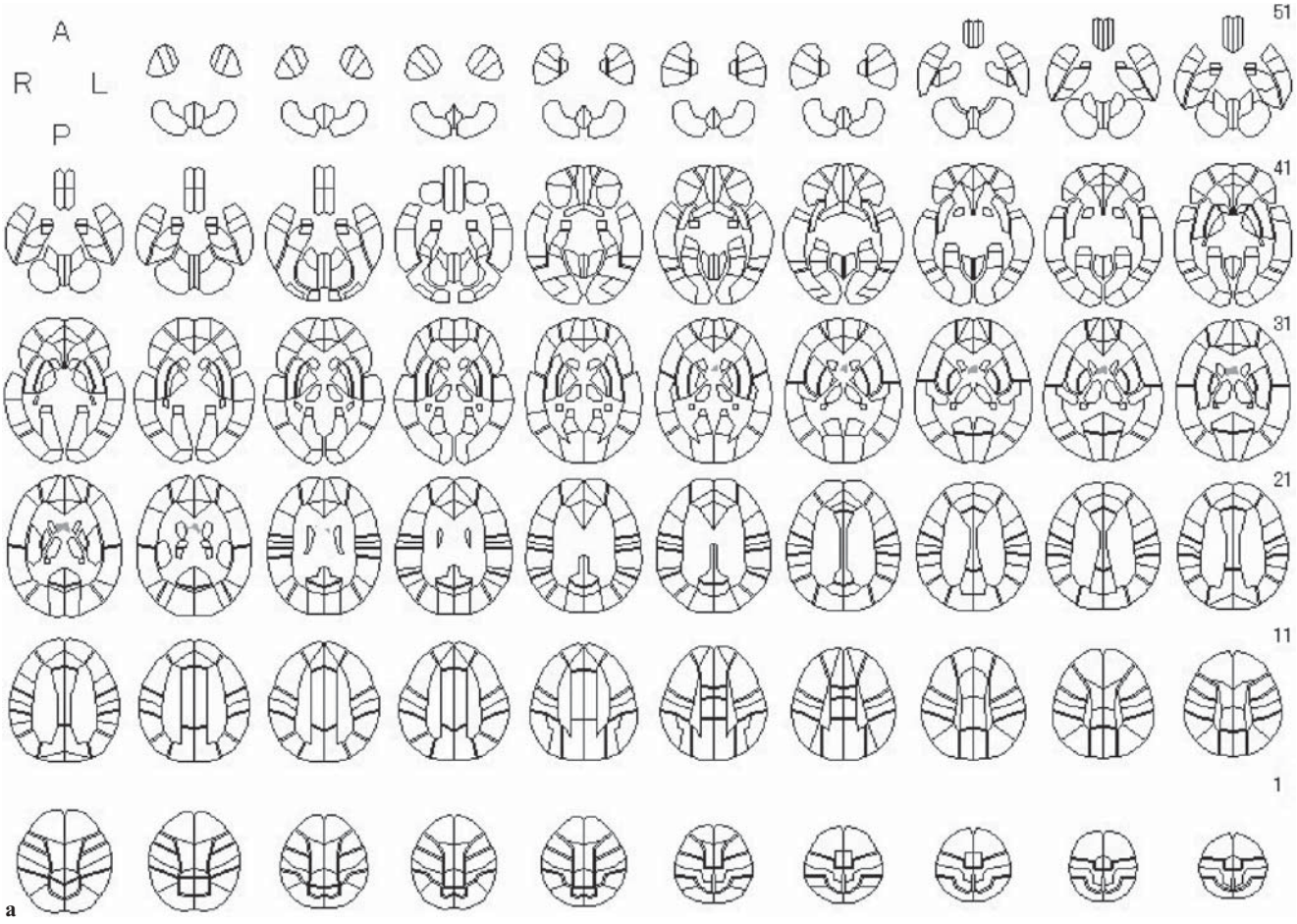


**Fig. 2.** **a** Constant 1394 ROIs (697 ROIs on each hemisphere) for the FineSRT. Each segment of the 3DSRT was subdivided into subsegments corresponding to respective cerebral convolutions. **b** Constant FineSRT ROI delineation on the $^{99m}$Tc-ethyl cysteinate dimer (ECD) template image. These images acted as the reference image for the anatomical standardization of $^{99m}$Tc-ECD single photon emission computed tomography (SPECT) images. The concordance between the constant ROI delineation and the template image was excellent

6. Temporal, 94 ROIs: superior temporal 34, middle temporal 35, inferior temporal 21, transverse temporal 4
7. Posterior cerebral, 106 ROIs; superior occipital 4, middle occipital 17, inferior occipital 8, lower precuneus 14, cuneus 23, lingual 15, parahippocampal 15, fusiform 10
8. Pericallosal, 31 ROIs; upper precuneus 11, cingulate 12, posterior cingulate 8
9. Basal ganglia, 50 ROIs; putamen 14, globus pallidus 8, caudate head 15, caudate tail 13
10. Thalamus, 10 ROIs
11. Hippocampus, 17 ROIs
12. Cerebellum, 43 ROIs: vermis 17, anterior lobe 13, posterior lobe 13
13. Extra, 25 ROIs: insula 17, amygdaloid body 8 (Fig. 2a)

## Imaging protocol

The imaging protocol has been described in a previously published article with the method shown in Fig. 3 used for the cerebral vascular reserve quantification (RVR method).[9,10]

Briefly, intravenous radionuclide angiography was performed by bolus injection of a half volume (1.5 ml) of the reconstituted $^{99m}$Tc-ethyl cysteinate dimer (ECD) (600 MBq/3 ml). Passage of the tracer from the aortic arch to the brain was monitored in a $128 \times 128$ format (magnification $\times 1.0$) for 120 s at 1-s intervals using a rectangular gamma camera of the two-head single photon emission computed tomography (SPECT) system (Prism 2000 XP; Picker International, Bedford Heights, OH, USA) equipped with high-resolution parallel-hole collimators. ROIs were placed manually over the aortic

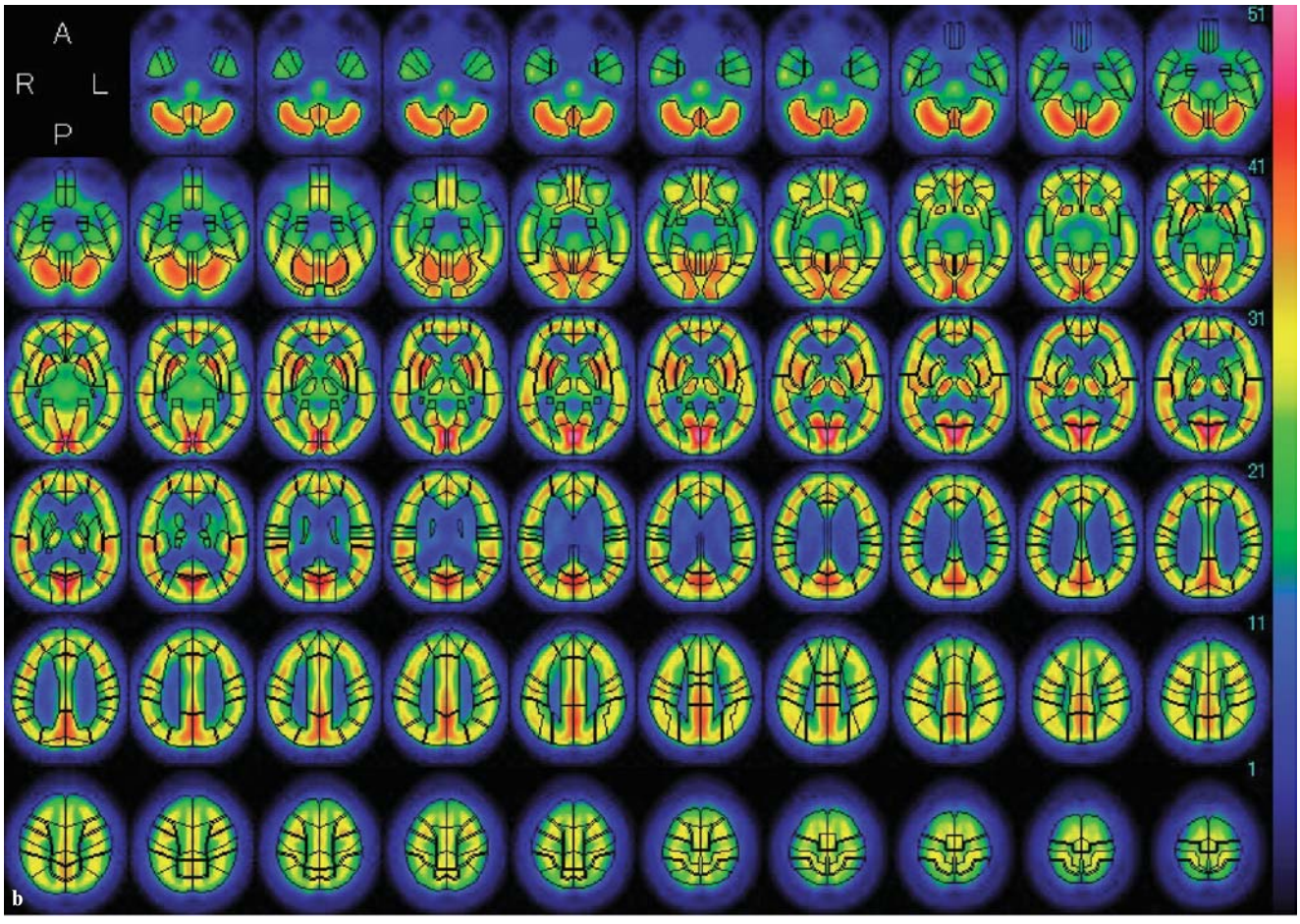


**Fig. 2.** *Continued*

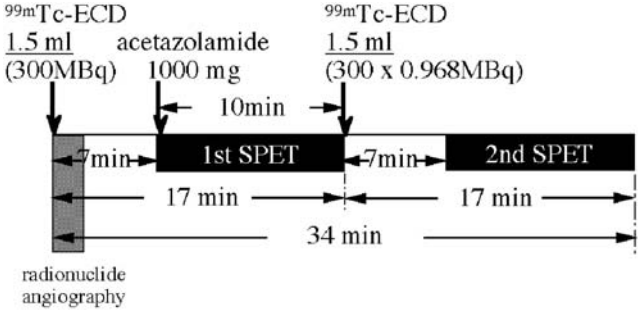


**Fig. 3.** Protocol of noninvasive, equal-volume-split $^{99m}$Tc-ECD consecutive SPECT method using acetazolamide (Acz) activation or the "vascular reserve quantification (RVR) method"

arch and bilateral cerebral hemispheres. Time activity curves of these two ROIs were plotted and the brain perfusion index (BPI) was determined as described previously.[11] BPI was then converted to the mean CBF (mCBF) value.[12]

Seven minutes after the completion of radionuclide angiography, cerebral SPECT imaging was carried out using the Prism 2000 XP employing high-resolution fan-beam collimators. The projection data were obtained in a 64 × 64 format (magnification ×1.33) for 30 angles in a 180° arc for each camera with 20 s per angle. The time required for SPECT data acquisition was 10 min. Acetazolamide (Acz) (1 g) was administered intravenously 10 min before completion of the first SPECT acquisition. Without any change in the patient's head position, the rest (1.5 ml) of the $^{99m}$Tc-ECD was administered immediately after the first data acquisition. Seven minutes later, the second SPECT acquisition was performed with acquisition conditions identical to those for the first scan. SPECT images were reconstructed by filtered back-projection using a Ramp filter followed by a post-processing Butterworth filter (order 8, cutoff 0.28). Attenuation correction was performed using Chang's method (attenuation coefficient: $\mu = 0.09$). To obtain Acz-activated (post-Acz) projection data, the first projection data were subtracted from the second SPECT data multiplied by 1.033, which was the correction coefficient for the decay of $^{99m}$Tc between the first and

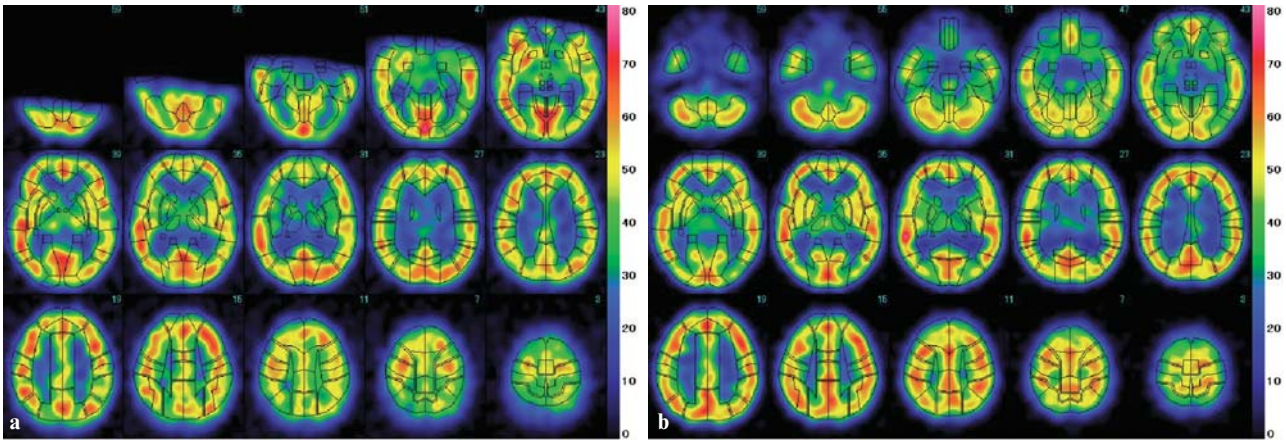


**Fig. 4.** **a** FineSRT results from the preoperative baseline cerebral blood flow (CBF) SPECT images of an 8-year-old girl with moyamoya disease. The inferior portion of the frontal cortex is out of the range of SPECT cameras because the distance from the shoulder to the skull base was too small. A difference between the right and left sides of the many gyri was appreciable. **b** FineSRT results from the post-EDAS baseline CBF SPECT images of the same girl at 14 years of age. All cerebral areas could be included in the image because she had matured during the 6-year interval. The preoperative difference disappeared

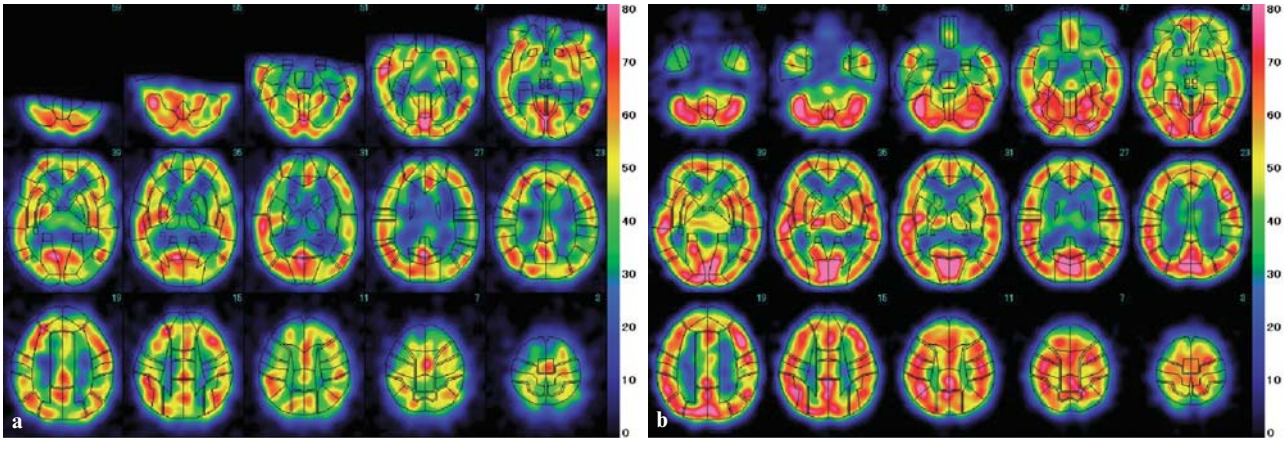


**Fig. 5.** **a** FineSRT results from the preoperative post-Acz CBF SPECT images of the 8-year-old girl with moyamoya disease. CBF was hardly increased after Acz administration in the bilateral hemisphere. **b** FineSRT results from the post-EDAS post-Acz CBF SPECT images of the same girl at 14 years of age. CBF was bilaterally increased after Acz administration. Response to Acz challenge was diffusely impaired in the bilateral hemispheres

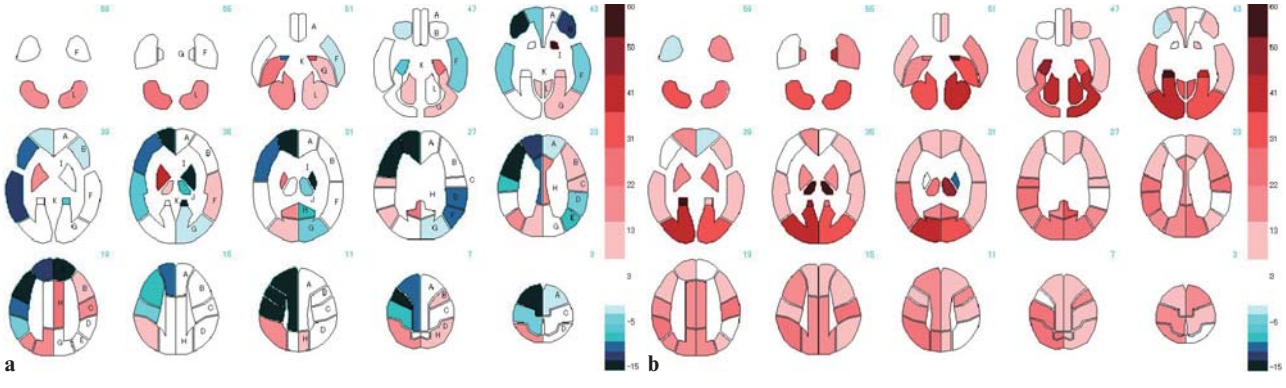


**Fig. 6.** **a** Percent increase map images drawn from the preoperative image: (post-Acz CBF—baseline CBF)/baseline CBF. This image is colored throughout each ROI with the respective percent increase value color according to the color scale. Increased and decreased segments are displayed in *red* and *blue* color gradations, respectively. The symbols are the same as in Fig. 1. Response to the Acz challenge was improved bilaterally. **b** Percent increase map images drawn from the postoperative image: (post-Acz CBF—baseline CBF)/ baseline CBF. Increased and decreased segments are displayed in the same *red* and *blue* color gradations as in **a**

**Table 1.** Summary of the results of a girl with Moyamoya disease analysed with FineSRT

| | Baseline sCBF | | | | Post-Acz sCBF | | | | Post-Acz sCBF/ Baseline sCBF | | | |
|---|---|---|---|---|---|---|---|---|---|---|---|---|
| | 8 Years old | | 15 Years old | | 8 Years old | | 15 Years old | | 8 Years old | | 15 Years old | |
| | Bilateral. 40.7 (ml/100 g per min) | | Bilateral. 42.6 (ml/100 g per min) | | Bilateral. 42.3 (ml/100 g per min) | | Bilateral. 51.0 (ml/100 g per min) | | Bilateral. 103.9 (%) | | Bilateral. 119.9 (%) | |
| Subsegment | Rt. | Lt. | Rt. | Lt. | Rt. | Lt. | Rt. | Lt. | Rt. | Lt. | Rt. | Lt. |
| Superior frontal | 38.6 | 39.4 | 39.0 | 40.1 | 32.3 | 35.2 | 43.7 | 42.9 | 83.7 | 89.3 | 112.2 | 107.1 |
| Medial frontal | 41.4 | 41.1 | 46.8 | 45.8 | 39.5 | 43.0 | 51.5 | 51.4 | 95.5 | 104.7 | 110.0 | 112.3 |
| Paracentral lobule | 42.8 | 42.3 | 52.6 | 50.8 | 42.3 | 45.2 | 58.9 | 60.5 | 98.7 | 106.7 | 111.8 | 119.2 |
| Anterior cingulate | 38.7 | 40.0 | 39.8 | 42.5 | 32.1 | 50.0 | 45.9 | 47.4 | 83.1 | 125.0 | 115.3 | 111.4 |
| Subcallosal | ND | ND | 37.2 | 40.0 | ND | ND | 42.7 | 47.4 | ND | ND | 114.9 | 118.4 |
| Orbital | ND | ND | 28.1 | 27.5 | ND | ND | 30.0 | 29.3 | ND | ND | 106.7 | 106.6 |
| Rectal | ND | ND | 33.5 | 33.3 | ND | ND | 36.3 | 37.5 | ND | ND | 108.3 | 112.5 |
| Middle frontal | 42.1 | 42.0 | 43.9 | 43.5 | 35.9 | 43.0 | 47.5 | 48.8 | 85.4 | 102.3 | 108.2 | 112.3 |
| Inferior frontal | 39.7 | 40.0 | 41.1 | 41.1 | 36.3 | 39.9 | 43.8 | 46.7 | 91.5 | 99.9 | 106.4 | 113.4 |
| Precentral | 43.6 | 43.4 | 42.4 | 43.9 | 38.6 | 43.3 | 51.8 | 51.3 | 88.5 | 99.6 | 122.3 | 117.0 |
| Postcentral | 42.6 | 41.1 | 42.8 | 43.7 | 39.8 | 43.0 | 49.6 | 50.1 | 93.3 | 104.6 | 115.8 | 114.6 |
| Insula | 43.8 | 44.2 | 43.0 | 43.4 | 50.8 | 45.6 | 52.9 | 49.8 | 116.1 | 103.2 | 122.9 | 114.8 |
| Superior parietal | 38.8 | 44.5 | 42.7 | 42.4 | 45.2 | 45.7 | 52.8 | 46.3 | 116.4 | 102.6 | 123.5 | 109.1 |
| Inferior parietal | 42.6 | 43.0 | 46.3 | 46.7 | 46.9 | 43.6 | 57.3 | 48.7 | 110.2 | 101.6 | 123.7 | 104.3 |
| Supramarginal | 47.2 | 42.5 | 43.1 | 43.4 | 44.0 | 39.6 | 56.0 | 43.9 | 93.2 | 93.0 | 129.9 | 101.2 |
| Angular | 45.2 | 49.7 | 48.1 | 47.8 | 53.3 | 47.8 | 58.2 | 54.1 | 117.8 | 96.2 | 121.2 | 113.3 |
| Superior temporal | 36.0 | 33.1 | 41.4 | 40.3 | 35.0 | 33.1 | 48.1 | 44.8 | 97.0 | 100.1 | 115.9 | 111.0 |
| Middle temporal | 36.3 | 35.2 | 41.3 | 40.8 | 36.9 | 33.5 | 48.5 | 46.2 | 101.6 | 95.2 | 117.5 | 113.2 |
| Inferior Temporal | 30.3 | 27.9 | 36.6 | 34.9 | 29.7 | 26.9 | 38.8 | 43.5 | 98.0 | 96.4 | 105.9 | 124.5 |
| Transverse Temporal | 44.8 | 49.4 | 49.3 | 51.4 | 59.0 | 49.8 | 60.4 | 53.2 | 131.5 | 100.8 | 122.5 | 103.6 |
| Superior occipital | 42.8 | 50.2 | 41.4 | 44.8 | 46.1 | 45.8 | 51.9 | 53.9 | 107.7 | 91.3 | 125.4 | 120.4 |
| Middle occipital | 43.3 | 46.7 | 39.3 | 37.2 | 43.4 | 44.8 | 52.5 | 49.8 | 100.2 | 95.9 | 133.5 | 134.1 |
| Inferior occipital | 41.9 | 41.2 | 40.7 | 36.7 | 38.3 | 41.4 | 54.4 | 52.8 | 91.4 | 100.5 | 133.5 | 144.0 |
| Precuneus (lower) | 46.3 | 47.2 | 54.7 | 52.9 | 53.2 | 48.6 | 64.7 | 63.6 | 114.8 | 103.0 | 118.2 | 120.0 |
| Cuneus | 45.6 | 48.4 | 46.7 | 45.6 | 48.6 | 46.8 | 64.5 | 62.4 | 106.6 | 96.7 | 138.1 | 136.9 |
| Hippocampus | 27.1 | 24.6 | 29.7 | 29.2 | 25.2 | 29.5 | 45.3 | 38.9 | 93.1 | 119.8 | 152.5 | 132.9 |
| Fusiform | 36.2 | 34.5 | 43.0 | 40.2 | 39.7 | 38.5 | 57.1 | 58.1 | 109.6 | 111.4 | 132.7 | 144.6 |
| Lingual | 45.7 | 43.3 | 44.7 | 45.5 | 52.2 | 47.5 | 61.8 | 59.1 | 114.3 | 109.6 | 138.3 | 129.9 |
| Parahippocampal | 25.0 | 21.1 | 34.5 | 34.5 | 26.4 | 23.8 | 47.8 | 45.3 | 105.3 | 112.7 | 138.5 | 131.2 |
| Amygdaloid body | 36.6 | 28.1 | 29.2 | 28.3 | 39.2 | 36.2 | 33.1 | 35.0 | 106.9 | 128.6 | 113.4 | 123.7 |
| Thalamus | 32.2 | 35.0 | 37.9 | 33.1 | 32.6 | 31.7 | 54.5 | 53.9 | 101.3 | 90.6 | 143.8 | 162.8 |
| Putamen | 41.3 | 40.7 | 44.0 | 43.9 | 47.0 | 39.6 | 49.8 | 49.6 | 113.6 | 97.3 | 113.2 | 112.9 |
| Globus Pallidus | 36.8 | 40.2 | 39.7 | 38.7 | 48.8 | 36.3 | 49.2 | 48.3 | 132.6 | 90.4 | 123.9 | 124.7 |
| Caudate head | 32.7 | 27.1 | 32.8 | 32.6 | 29.1 | 29.0 | 36.6 | 33.3 | 89.1 | 106.9 | 111.6 | 102.1 |
| Caudate tail | 21.6 | 22.6 | 26.0 | 22.4 | 23.9 | 26.1 | 35.1 | 26.9 | 110.4 | 115.3 | 134.9 | 120.0 |
| Precuneus (upper) | 44.5 | 44.8 | 48.9 | 49.8 | 45.8 | 45.5 | 58.9 | 58.0 | 103.0 | 101.5 | 120.3 | 116.6 |
| Cingulate | 41.8 | 40.9 | 40.1 | 40.9 | 41.6 | 47.9 | 47.1 | 48.4 | 99.5 | 116.9 | 117.4 | 118.2 |
| Posterior cingulate | 42.8 | 42.6 | 41.6 | 38.7 | 52.1 | 42.2 | 51.8 | 49.0 | 121.5 | 99.2 | 124.6 | 126.6 |
| Vermis | 51.0 | 52.5 | 46.0 | 47.2 | 58.4 | 53.2 | 57.9 | 60.7 | 114.6 | 101.3 | 125.8 | 128.7 |
| Anterior lobe | 46.0 | 45.8 | 39.0 | 40.1 | 51.7 | 48.5 | 53.2 | 56.4 | 112.5 | 105.8 | 136.3 | 140.6 |
| Posterior lobe | 42.9 | 39.2 | 49.4 | 48.6 | 51.4 | 45.2 | 65.4 | 65.0 | 120.0 | 115.2 | 132.5 | 133.6 |

Values after "Bilateral" are bilateral mean value.
sCBF, subsegmental CBF; Post-Acz, acetazolamide-activated; ND, not detected

second SPECT studies. Finally, the baseline and post-Acz projection data were reformatted to construct transaxial images parallel to the orbitomeatal line. The pixel size and the slice thickness were 4.5 mm$^2$ and 4.5 mm, respectively. Baseline and post-Acz $^{99m}$Tc-ECD transaxial SPECT images were consequently converted to baseline and the post-Acz quantitative rCBF images by application of Lassen's linearization correction algorithm ($\alpha$ = 2.59).[13] These images were analyzed using 3DSRT and FineSRT.

## Case report

An 8-year-old girl with occlusion in the bilateral internal carotid arteries and compensatory collateral moyamoya vessels underwent bilateral encephaloduroarteriosynangiosis (EDAS). The baseline and post-Acz quantitative CBF SPECT images were obtained before and 6 years after EDAS using the RVR method. These images were analyzed with 3DSRT and FineSRT using a $^{99m}$Tc-ECD template image (shown in Fig. 2b). An appreciable difference between the right and left sides of the many gyri (especially in the superior parietal gyrus, angular gyrus, superior occipital gyrus, and caudate head) on the preoperative baseline CBF SPECT image (Fig. 4a) had disappeared on the postoperative studies (Fig. 4b), as shown in Table 1. More strikingly, vascular reserve impairment widely recognized in the preoperative study had markedly improved after the operation (Figs. 5, 6, Table 1).

## Discussion

Our fully automated software applied the constant ROIs on the anatomically standardized cerebral images, which shared common anatomical architecture defined in the MNI space of the SPM. Consequently, CBF SPECT images could be compared without consideration of brain outline. Therefore, it is thought that the software will greatly contribute to the analysis of pediatric CBF SPECT images. As shown in the presented case, the size and shape of the brain changed considerably the follow-up period, but precise estimation could be easily performed using the FineSRT software.

FineSRT was useful for analyzing perfusion conditions, although in some studies the obtained information for each gyrus was too complicated. Instead, because of the lower ROI number of 3DSRT being about 45% of those of FineSRT, the 3DSRT could provide information for each area perfused by the respective primary branch of the cerebral arteries. Moreover, 3DSRT could display a "map image," colored throughout each ROI with the respective average count color according to the color scale, as presented in Fig. 6. The map image, although it is only a diagram, can be easily drawn by 3DSRT; and it seems particularly helpful in the visual assessment of cerebral perfusion.

Finally, we must mention that, regrettably, we are just starting the positron emission tomography (PET) analysis, but template images using SPM with miscellaneous SPECT or PET tracers have already been provided. Thus, it is expected that the applicability of our methodology will soon be useful for constant ROI quantification of $^{15}$O and $^{18}$F PET data as well.

*Note*: If anyone is interested in the 3DSRT and FineSRT software, it is free. Please contact us by e-mail (3dsrt@drl.co.jp).

## References


1. Friston KJ, Frith CD, Liddle PF, Frackowiak RS. Comparing functional (PET) images: the assessment of significant change. J Cereb Blood Flow Metab 1991;11:690–9.
2. Friston KJ, Holmes AP, Worsely KJ, Poline JP, Frith CD, Frackowiak RS. Statistical parametric maps in functional imaging: a general linear approach. Hum Brain Mapp 1995;2: 189–210.
3. Minoshima S, Frey KA, Koeppe RA, Foster NL, Kuhl DE. A diagnostic approach in Alzheimer's disease using three-dimensional stereotactic surface projections of fluorine-18-FDG PET. J Nucl Med 1996;36:1238–48.
4. Takeuchi R, Yonekura Y, Matsuda H, Konishi J. Usefulness of a three-dimensional stereotaxic ROI template on anatomically standardised $^{99m}$Tc-ECD SPET. Eur J Nucl Med 2002;29: 331–41.
5. Takeuchi R, Yonekura Y, Katayama S, Takeda N, Fujita J, Konishi J. Fully automated quantification of regional cerebral blood flow with three-dimensional stereotaxic region of interest template: validation using magnetic resonance imaging: technical note. Neurol Med Chir (Tokyo) 2003;43:153–62.
6. Takeuchi R, Matsuda H, Yoshioka K, Yonekura Y. Cerebral blood flow SPET in transient global amnesia with automated ROI analysis by 3DSRT. Eur J Nucl Med Mol Imaging 2004; 31:578–89.
7. Takeuchi R. Atlas of the constant regions of interest on the brain anatomically standardized by SPM. Tokyo: Kyohritsu; 2005. p. 1–101.
8. Salmond CH, Ashbumer J, Vargha-Khadem F, Gadian DG, Friston KJ. Detecting bilateral abnormalities with voxel-based morphometry. Hum Brain Mapp 2000;11:223–32.
9. Takeuchi R, Matsuda H, Yonekura Y, Sakahara H, Konishi J. Noninvasive quantitative measurements of regional cerebral blood flow using technetium-99m-L,L-ECD SPECT activated with acetazolamide: quantification analysis by equal-volume-split $^{99m}$Tc-ECD consecutive SPECT method. J Cereb Blood Flow Metab 1997;17:1020–32.
10. Takeuchi R, Yonekura Y, Matsuda H, Nishimura Y, Tanaka H, Ohta H, et al. Resting and acetazolamide-challenged technetium-99m-ECD SPECT in transient global amnesia. J Nucl Med 1998;39:1360–2.
11. Matsuda H, Tsuji S, Shuke N, Sumiya H, Tonami N, Hisada K. A quantative approach to technetium-99m hexamethylpropylene amine oxime. Eur J Nucl Med 1992;19: 195–200.
12. Matsuda H, Yagishita A, Tsuji S, Hisada K. A quantitative approach to technetium-99m ethyl-cysteinate dimer: a comparison with hexamethylpropylene amine oxime. Eur J Nucl Med 1995;22:633–7.
13. Lassen NA, Andersen AR, Friberg L, Paulson OB. The retention of [$^{99m}$Tc]-d,l,-HM-PAO in the human brain after intracarotid bolus injection: a kinetic analysis. J Cereb Blood Flow Metab 1988;8(Suppl 1):13–22.